



# The concept of event-size dependent exhaustion and its application to paraglacial rockslides

Stefan Hergarten<sup>1</sup>

<sup>1</sup>Institut für Geo- und Umweltnaturwissenschaften, Albert-Ludwigs-Universität Freiburg, Albertstr. 23B, 79104 Freiburg, Germany

**Correspondence:** Stefan Hergarten  
(stefan.hergarten@geologie.uni-freiburg.de)

**Abstract.** Rockslides are a major hazard in mountainous regions. In formerly glaciated regions, the disposition mainly arises from oversteepened topography and decreases through time. However, little is known about this decrease and thus about the present-day hazard of huge, potentially catastrophic rockslides. This paper presents a new theoretical concept that combines the decrease in disposition with the power-law distribution of rockslide volumes found in several studies. The concept starts from a given initial set of potential events, which are randomly triggered through time at a probability that depends on event size. The developed theoretical framework is applied to paraglacial rockslides in the European Alps, where available data allow for constraining the parameters reasonably well. The results suggest that the probability of triggering increases roughly with the cube root of the volume. For small rockslides up to 1000 m<sup>3</sup>, an exponential decrease of the frequency with an *e*-folding time longer than 65,000 yr is predicted. In turn, the predicted *e*-folding time is shorter than 2000 yr for volumes of 10 km<sup>3</sup>, so that the occurrence of such huge rockslides is unlikely at present times. For the largest rockslide possible at present times, a median volume of 0.5 to 1 km<sup>3</sup> is predicted. With a volume of 0.27 km<sup>3</sup>, the artificially triggered rockslide that hit the Vaiont reservoir in 1963, is thus not extraordinarily large. Concerning its frequency of occurrence, however, it can be considered a 700 to 1200-year event.

## 1 Introduction

Rockslides are a ubiquitous hazard in mountainous regions. The biggest rockslide in the European Alps since 1900 took place in 1963 at the Vaiont reservoir. It involved a volume of about 0.27 km<sup>3</sup>. Owing to an overtopping of the dam, it claimed more than 2000 lives. However, the reservoir played an important part in triggering this huge rockslide, so that it cannot be considered a natural event. The largest natural rockslides in the Alps since 1900 are considerably smaller (e.g., Gruner, 2006).

In turn, two huge rockslides with volumes of several cubic kilometers have been identified and dated. These are the Flims rockslide with a deposited volume of about 10 km<sup>3</sup> (Aaron et al., 2020) in the carbonatic rocks of the Rhine valley and the Köfels rockslide with a deposited volume of about 4 km<sup>3</sup> (Zangerl et al., 2021) in the crystalline rocks of the Oetz valley. Estimates of the ages of these two giant events scatter by some 100 years (Deplazes et al., 2007; Nicolussi et al., 2015, and references therein). Within this scatter, however, both ages are about 9500 BP. These ages refute the older idea of triggering by glacial debuttressing. Since the inner Alpine valleys were largely free of ice at about 18,000 BP (e.g., Ivy-Ochs et al., 2008),



25 an immediate relation to the deglaciation of the respective valleys can be excluded. Consequently, von Poschinger et al. (2006) concluded that rockslides of several cubic kilometers have to be taken into consideration also at present.

Although an immediate effect of deglaciation can be excluded, the former glaciation of the valleys plays a central part for rockslide disposition. In the context of paraglacial rock-slope failure, Cruden and Hu (1993) proposed the concept of exhaustion (see also Ballantyne, 2002a, b). The concept is similar to radioactive decay. Starting from an initial population of potentially  
30 unstable sites, it is assumed that each of them is triggered at a given probability per time  $\lambda$ . Then both the remaining number of potentially unstable sites and the rockslide frequency decrease like  $e^{-\lambda t}$ . Analyzing a small data set of 67 rockslides with volumes  $V \geq 1000 \text{ m}^3$  in the Canadian Rocky Mountains, where 14 similar potentially unstable sites were found, Cruden and Hu (1993) estimated  $\lambda = 0.18 \text{ kyr}^{-1}$ , equivalent to an  $e$ -folding time  $T = \lambda^{-1} = 5700 \text{ yr}$ .

As a main limitation, however, the estimate  $T = 5700 \text{ yr}$  refers to the total number of rockslides with  $V \geq 1000 \text{ m}^3$ . Whether  
35 this estimate could be transferred to rockslides of any given size is nontrivial. If this result could be transferred to rockslides of any size in the Alps, the present-day probability even of huge rockslides would be only by a factor of  $e^{\frac{9500}{5700}} \approx 5$  lower than it was at the time of the Flims and K ofels rockslides.

Analyzing the statistical distribution of landslide sizes became popular a few years later than the concept of exhaustion was proposed, presumably pushed forward by the comprehensive analysis of several thousand landslides in Taiwan by Hovius  
40 et al. (1997). Reanalyzing several data sets, Malamud et al. (2004) found that landslides in unconsolidated material as well as rockfalls and rockslides follow a power-law distribution over some range in size. The exponent of the power law was found to be independent of the triggering mechanism (e.g., earthquakes, rainstorms or rapid snow melt), but is considerably lower for rockfalls and rockslides than for landslides in unconsolidated material. The distinct dependence on the material was confirmed by Brunetti et al. (2009). For deeper insights into the scaling properties of landslides, the review article of Tebbens (2020) is  
45 recommended.

Several models addressing the power-law distribution of landslides were developed so far (Densmore et al., 1998; Hergarten and Neugebauer, 1998; Hergarten, 2012; Alvioli et al., 2014; Liucci et al., 2017; Jeandet et al., 2019; Campforts et al., 2020). Some of these studies discussed landslides in the context of self-organized criticality (SOC). The idea of SOC was introduced by Bak et al. (1987) and promised to become a unifying theoretical concept for dynamic systems that generate events of various  
50 sizes following a power-law distribution. Jensen (1998) characterized SOC systems as slowly driven, interaction-dominated threshold systems. In the context of landslides, relief is generated directly or indirectly (e.g., in combination with fluvial incision) by tectonics. This process is rather continuous and slow. In turn, landslides take place as discrete events if a threshold is exceeded and consume relief. A system that exhibits SOC approaches some kind of long-term equilibrium between the two  
processes with power-law distributed event sizes.

55 Now the question arises how the idea of paraglacial exhaustion can be reconciled with the power-law distribution of rockslide sizes, perhaps in combination with SOC. While size distributions of rockfalls and rockslides were addressed in several studies during the previous decade (e.g., Bennett et al., 2012; Lari et al., 2014; Valagussa et al., 2014; Strunden et al., 2015; Tanyas et al., 2018; Hartmeyer et al., 2020; Mohadjer et al., 2020), only the two latest studies refer directly to paraglacial exhaustion. Mohadjer et al. (2020) attempted to estimate the total volume of rockfalls in a deglaciated valley at different time scales up to



60 11,000 yr. In turn, Hartmeyer et al. (2020) investigated the rockfall activity at walls above a retreating glacier at much smaller spatial and temporal scales.

In this paper, a theoretical framework for event-size-dependent exhaustion is developed, which means that the decay constant  $\lambda$  depends on the event size. In the following section, it is illustrated that the Drossel-Schwabl forest-fire model as one of the simplest models in the field of SOC already predicts such a behavior. In Sect. 3, the theoretical framework will be developed.

65 This framework will be applied to the Alps in Sect. 4, and it will be investigated to what extent the sparse available data on large rockslides can be used to constrain the parameters.

## 2 Motivation: The Drossel-Schwabl forest-fire model

Let us start with the Drossel-Schwabl forest-fire model (DS-FFM in the following) as an example. While several in their spirit similar models were developed soon after the idea of SOC became popular, the version proposed by Drossel and Schwabl  
70 (1992) with a simplification introduced by Grassberger (1993) attracted the greatest interest. Although obviously oversimplified, it was found later that it reproduces some properties of real wildfires quite well (Malamud et al., 1998; Zinck and Grimm, 2008; Krenn and Hergarten, 2009).

The DS-FFM is a stochastic cellular automaton model that is usually considered on a two-dimensional square lattice with periodic boundary conditions. Each site can be either empty or occupied by a tree. In each time step, a given number  $\theta$  of  
75 new trees is planted at randomly selected sites, assuming that planting a tree at an already occupied site has no effect. Then a randomly selected site is ignited. If this site is occupied by a tree, this tree and the entire cluster of connected trees are burned. By default, only nearest-neighbor connections are considered.

Regardless of the initial condition, the DS-FFM self-organizes towards a quasi-steady state in which as many trees are burned as are planted on average. If the growth rate  $\theta$  and the size of the model are sufficiently large, about 40 % of all sites  
80 are occupied on average and the distribution of the fire sizes roughly follows a power law. The DS-FFM was investigated numerically and theoretically in numerous studies (e.g., Christensen et al., 1993; Henley, 1993; Clar et al., 1994; Pastor-Satorras and Vespignani, 2000; Pruessner and Jensen, 2002; Schenk et al., 2002; Hergarten and Krenn, 2011), resulting in a more or less complete understanding of its properties.

Let us now assume that the growth of new trees ceases suddenly at some time in the quasi-steady state, so that the available  
85 clusters of trees are burned successively. Figure 1 shows an example computed on a small grid of  $256 \times 256$  sites with  $\theta = 100$ . It is immediately recognized that the largest fires take place quite early. This property is owing to the the mechanism of ignition. Each cluster of trees can be burned equivalently by igniting any of its trees. So the probability that a cluster of trees is burned is proportional to the cluster size (number of trees). This implies that large clusters are preferred to small clusters at any time. This property was already used by Hergarten and Krenn (2011) for deriving a semi-phenomenological explanation of the power-law  
90 distribution in the quasi-steady state and by Krenn and Hergarten (2009) for modifying the DS-FFM towards human-induced fires.

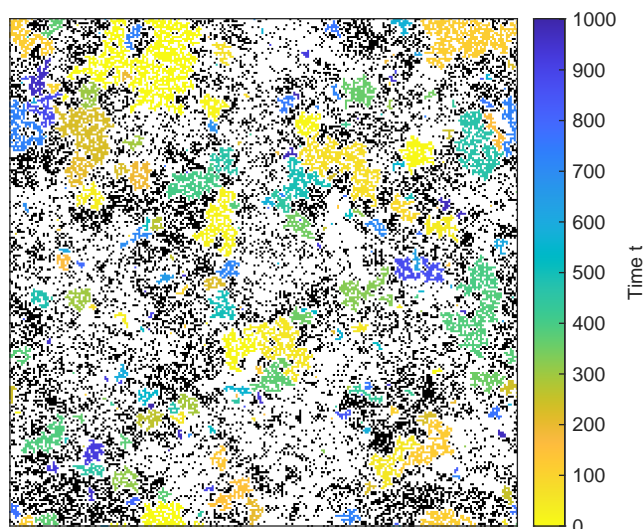


**Figure 1.** Burned clusters of trees without regrowth on a  $256 \times 256$  grid. One unit of time corresponds to one event of ignition. Colored patches correspond to clusters burned at different times. White sites were already empty in the beginning, while black clusters are still present after the simulated 1000 events of ignition.

Owing to the preference of large fires, the DS-FFM in a phase without regrowth is an example of event-size dependent exhaustion. Figure 2 shows the size distribution of the fires derived from a simulation on a larger grid of  $65,536 \times 65,536$  sites with  $\theta = 10,000$ . It is immediately recognized that the distribution derived from the quasi-steady state (black curve) follows a power law only over a limited range with an excess of fires with sizes  $s \approx 10^5$  and a rapid decline at larger sizes. While this behavior was explained by Hergarten and Krenn (2011), the excess below the rapid decline is not relevant here.

The distribution of the fires that take place during the first 10,000 steps after growth has ceased is almost identical to the distribution in the quasi-steady state. A small deficit is only visible at the tail. So the overall consumption of clusters during the first 10,000 steps is negligible, except for the largest clusters. The trend that large clusters are consumed more rapidly than small clusters is consolidated over larger time spans. As an example, the frequency of fires with sizes  $s \approx 10^5$  is in the time interval from  $t = 10^5$  to  $10^6$  by more than two decades lower than in the quasi-steady state, while the frequency of fires with  $s \lesssim 10^3$  is still almost unaffected.

As a central result, the power-law distribution of the fires is consumed through time from the tail. In particular, the exponent (slope in the double-logarithmic plot) stays the same in principle, while only the range of the power law becomes shorter. Finally, however, the decay also affects the frequency of the smallest fires.

### 3 Theoretical framework

Let us assume that the process of exhaustion starts at  $t = 0$  from a given set of objects (potential events) described by a nondimensional size  $s$ . This size is defined in such a way that the probability of decay (generating an event) per time is

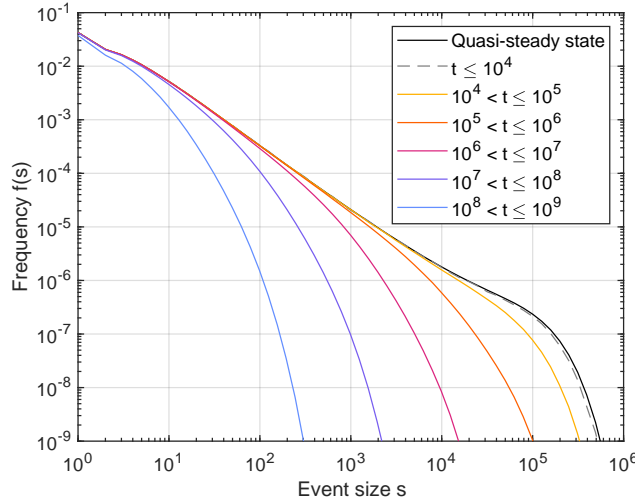


**Figure 2.** Frequency of the fires in the DS-FFM during phases without growing trees. All distributions were obtained from simulations on a  $65,536 \times 65,536$  grid with  $\theta = 10,000$  and smoothed by logarithmic binning with 10 bins per decade. The black curve describes the frequency of fires per ignition event in the quasi-steady state, while the other curves describe different time slices. These data were obtained by stacking 75 simulated sequences starting from different points of the quasi-steady state.

proportional to  $s$  (as in the DS-FFM),

$$110 \quad \lambda(s) = \mu s, \tag{1}$$

with a given value  $\mu$ . Then the frequency density  $\phi(s, t)$  of the objects still there at time  $t$  decreases according to

$$\frac{\partial}{\partial t} \phi(s, t) = -\lambda(s)\phi(s, t) = -\mu s \phi(s, t). \tag{2}$$

This leads to

$$\phi(s, t) = \phi(s, 0)e^{-\mu s t}, \tag{3}$$

115 where  $\phi(s, 0)$  is the initial frequency density of the objects.

Let us further assume that the objects initially follow a power-law (Pareto) distribution, which is most conveniently written in the cumulative form

$$\Phi(s, 0) = n s^{-\alpha} \tag{4}$$

with an exponent  $\alpha$ . The cumulative frequency  $\Phi(s, t)$  describes the expected number of objects with sizes greater than or equal to  $s$  at time  $t$ . Accordingly,  $n$  is the initial number of objects with sizes  $s \geq 1$ . The respective frequency density is

$$120 \quad \phi(s, 0) = -\frac{\partial}{\partial s} \Phi(s, 0) = n \alpha s^{-\alpha-1}, \tag{5}$$



which yields

$$\phi(s, t) = \phi(s, 0)e^{-\mu st} = n\alpha s^{-\alpha-1}e^{-\mu st} \tag{6}$$

in combination with Eq. (3).

125 Computing the cumulative frequency  $\Phi(s, t)$  requires the integration of Eq. (6):

$$\Phi(s, t) = \int_s^\infty \phi(\sigma, t) d\sigma = \int_s^\infty n\alpha \sigma^{-\alpha-1} e^{-\mu \sigma t} d\sigma. \tag{7}$$

Substituting  $u = \mu \sigma t$ , the integral can be transformed into

$$\Phi(s, t) = n\alpha (\mu t)^\alpha \int_{\mu st}^\infty u^{-\alpha-1} e^{-u} du = n\alpha (\mu t)^\alpha \Gamma(-\alpha, \mu st) \tag{8}$$

with the upper incomplete gamma function

$$130 \Gamma(e, x) = \int_x^\infty u^e e^{-u} du. \tag{9}$$

The negative rate of change in  $\phi(s, t)$  defines the frequency density of the events per unit time,

$$f(s, t) = -\frac{\partial}{\partial t} \phi(s, t) = \mu s \phi(s, t) = n\mu \alpha s^{-\alpha} e^{-\mu st}. \tag{10}$$

The respective cumulative frequency of the events per unit time,  $F(s, t)$ , can be computed by performing the same steps as in Eqs. (7) and (8):

$$135 F(s, t) = \int_s^\infty f(\sigma, t) d\sigma = n\mu \alpha (\mu t)^{\alpha-1} \Gamma(1 - \alpha, \mu st). \tag{11}$$

As an example, Fig. 3 shows the respective distributions for  $\alpha = 1.2$  and  $\mu = 1$ . The two frequency densities  $f(s, t)$  and  $\phi(s, t)$  are still close to the respective initial densities at  $t = 10^{-3}$  over a considerable range of sizes. Their exponents differ by one ( $\alpha$  vs.  $\alpha + 1$ ). According to Eqs. (3) and (10), the actual frequency density drops below the respective power law by a factor of  $e$  at a size

$$140 s_c = \frac{1}{\mu t}, \tag{12}$$

which can be used for characterizing the transition from a power law to an exponential decay. In this example,  $s_c = 1000$  at  $t = 10^{-3}$ .

For the cumulative frequencies, the deviations from the respective power law extend towards smaller sizes compared to the frequency densities. The stronger deviation arises from the dependence of the cumulative frequency at size  $s$  on the frequency density of all greater sizes.

145

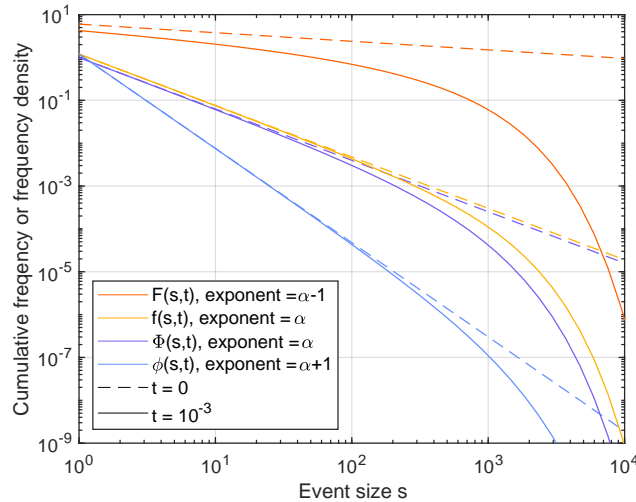


**Figure 3.** Cumulative frequency and frequency density of the events per unit time ( $F(s, t)$ ,  $f(s, t)$ ) and the objects still present ( $\Phi(s, t)$ ,  $\phi(s, t)$ ) at  $t = 0$  and  $t = 10^{-3}$  for  $\alpha = 1.2$  and  $\mu = 1$ . All distributions were normalized to the total number  $n$  of objects with sizes  $s \geq 1$  ( $n = 1$  in all equations).

#### 4 Application to paraglacial rockslides in the Alps

Applying the framework developed in Sect. 3 to paraglacial rockslides in a given region requires the definition of the event size  $s$  in the sense of Eq. (1) at first. This means that the probability of failure at a potential rockslide site is proportional to  $s$ . In contrast to the DS-FFM considered in Sect. 2, defining  $s$  is not straightforward here. Let us assume a general power-law relation

$$s = \left( \frac{V}{V_0} \right)^\gamma \tag{13}$$

with a given exponent  $\gamma$  and a reference volume  $V_0$ . Then  $\mu$  (Eq. 1) is the decay constant  $\lambda$  for rockslides with a volume  $V = V_0$  and  $n$  (Eq. 4) the initial number of potential rockslide sites with  $V \geq V_0$ .

It should be expected that  $\gamma \leq 1$ . As an example, assuming that failure can be initiated at each point of the fracture surface at the same probability and that the detached body of rock scales with size isotropically leads to  $\gamma = \frac{2}{3}$ . Alternatively, assuming that failure starts only from points at the outcrop of the fracture surface (so the perimeter) would result in  $\gamma = \frac{1}{3}$ .

So forward modeling based on the concept of size-dependent exhaustion involves the four parameters  $\gamma$ ,  $\mu$ ,  $\alpha$ , and  $n$ . When referring to real-world data, however, it is not known when the process of exhaustion started. Therefore, a real-world time  $t_0$  must be assigned to the starting point  $t = 0$  used in the theoretical framework, which introduces an additional parameter.

Since data on the frequency of rockslides are sparse and the completeness of inventories is often an issue, validating the exhaustion model and constraining its parameters is challenging. For the European Alps as a whole, a combination of historical and prehistorical data is used in the following.





1. 18 rockslides with volumes between  $10^6$  and  $10^7$  m<sup>3</sup> took place from 1850 to 2020 CE. These are 15 events until 2000 CE reported by Gruner (2006) and 3 events in the 21<sup>th</sup> century (Dents du Midi, 2006; Bondo 2011 and 2017).
- 165 2. 7 rockslides with volumes between  $10^7$  and  $10^8$  m<sup>3</sup> took place from 1850 to 2020 CE (Gruner, 2006).
3. 2 rockslides with volumes greater than  $10^8$  m<sup>3</sup> took place from 1000 to 2020 CE (Gruner, 2006).
4. At  $t = 9450$  BP, the largest potential rockslide volume is 10 km<sup>3</sup>, corresponding to age (Deplazes et al., 2007) and volume (Aaron et al., 2020) of the Flims rockslide.
5. At  $t = 9500$  BP, the second-largest potential rockslide volume is 4 km<sup>3</sup>, corresponding to age (Nicolussi et al., 2015) and volume (Zangerl et al., 2021) of the Köfels rockslide.
- 170 6. At  $t = 3210$  BP, the largest potential rockslide volume is 1.1 km<sup>3</sup>, corresponding to the Kandersteg rockslide (Singeisen et al., 2020).
7. At  $t = 4150$  BP, the second-largest potential rockslide volume is 1 km<sup>3</sup>, corresponding to the Fernpass rockslide (Gruner, 2006).

175 Anthropogenically triggered rockslides were not taken into account in these data.

The data 4–7 differ from the data 1–3 since they are not inventories over a given time span, but refer to the largest or second-largest available volumes at a given time. The respective statistical distributions are described by rank-ordering statistics (e.g., Sornette, 2000, Chapter 6). A maximum likelihood approach that combines both types of data is presented in Appendix A.

However, the 7 constraints defined above provide a very limited basis for constraining the 5 parameters  $\gamma$ ,  $\mu$ ,  $\alpha$ ,  $n$ , and  $t_0$ .  
180 Since these constraints refer to volumes  $V \geq 10^6$  m<sup>3</sup>, it would be useful to include information about smaller events from local inventories. As exhaustion predominantly affects the frequency of large events, it makes sense to assume that the power-law distribution typically found in local inventories defines the initial distribution, so that the initial frequency density  $f(s, 0)$  of the events follows a power law with the exponent  $\alpha$  (Eq. 10). As reviewed by Brunetti et al. (2009), this exponent is typically in the range  $\alpha_V \in [1.1, 1.4]$ , where the subscript V indicates that this value refers to volume instead of the generic measure of  
185 event size  $s$ . The relation between  $\alpha_V$  and  $\alpha$  is easily obtained from the cumulative frequency of the events at  $t = 0$ ,

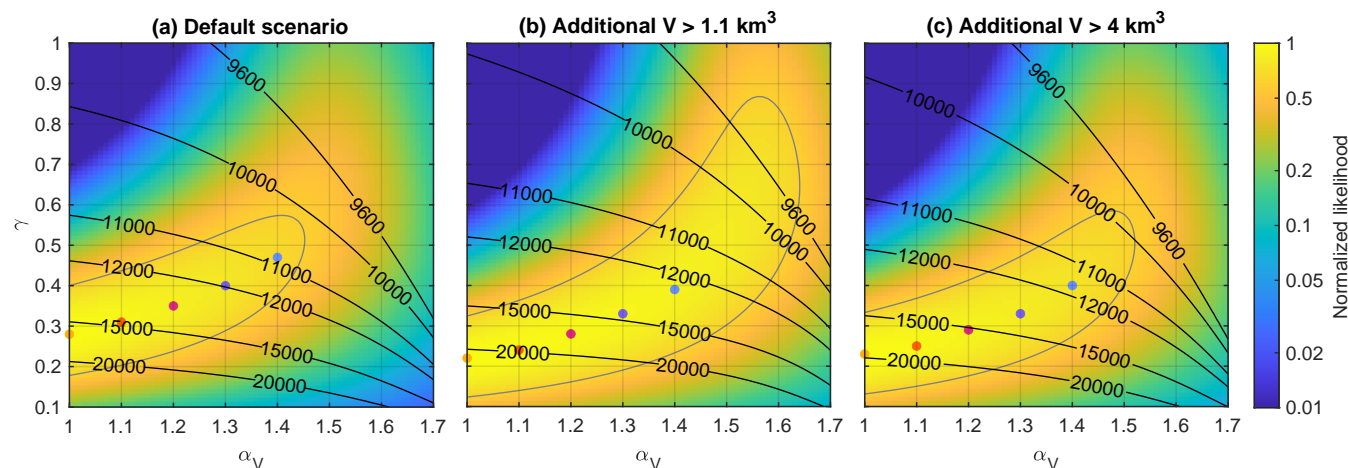
$$F(s, 0) \propto s^{-(\alpha-1)} \propto V^{-\gamma(\alpha-1)} = V^{-(\alpha_V-1)} \quad (14)$$

with

$$\alpha_V = \gamma(\alpha - 1) + 1. \quad (15)$$

While  $\alpha_V$  is used instead of  $\alpha$  in the following, knowledge about  $\alpha_V$  from real-world inventories is not directly included in the maximum likelihood approach. The typical range  $\alpha_V \in [1.1, 1.4]$  is only used for checking whether the estimate obtained from  
190 the maximum likelihood approach is consistent with local inventories.





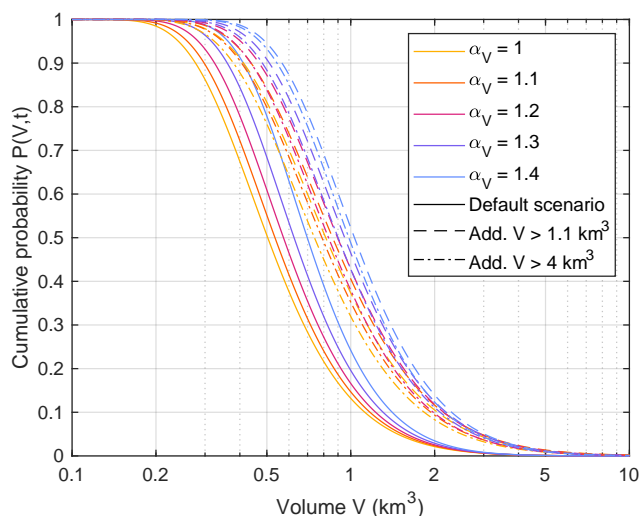
**Figure 4.** Likelihood as a function of  $\alpha_V$  and  $\gamma$  for different scenarios. The maximum likelihood values taken over all combinations of the remaining parameters  $\mu$ ,  $n$ , and  $t_0$  are shown. Likelihood values are normalized to the maximum value, and the gray contour line refers to  $e^{-0.5} \approx 0.61$  of the maximum likelihood. Black contour lines describe the obtained time  $t_0$  (BP) at which the process of exhaustion started. Colored dots refer to the points with the highest likelihood for  $\alpha_V = 1, 1.1, 1.2, 1.3$  and  $1.4$ .

Figure 4a shows the likelihood as a function of the exponents  $\alpha_V$  and  $\gamma$ . Since absolute values of the likelihood have no immediate meaning, all values are normalized to the maximum values. The highest likelihood is even achieved for  $\alpha_V = 1$  in combination with  $\gamma = 0.28$ . However, the likelihood increases only by a factor of 0.68 for  $\alpha_V = 1.4$  and  $\gamma = 0.47$ . For a Gaussian likelihood function, the standard deviation would correspond to a reduction by a factor of  $e^{-0.5} \approx 0.61$ , which is marked by the gray contour line. So the entire parameter region inside the gray line cannot be considered unlikely.

Qualitatively, however, the observed increase in likelihood towards smaller exponents  $\alpha_V$  makes sense. Since size-dependent exhaustion particularly reduces the frequency of large events, it may introduce a bias towards larger estimates of  $\alpha_V$  in rockslide inventories compared to the initial distribution, so the real value of  $\alpha_V$  may be rather at the lower edge of the observed interval  $\alpha_V \in [1.1, 1.4]$  or even be slightly below 1.1.

In addition to the default scenario based on the 7 constraints defined above, Fig. 4 also shows the results of two alternative scenarios. These scenarios challenge the assumption that the Kandersteg rockslide was the largest potential rockslide at its time. In Fig. 4b, it is assumed that there was one more potential event larger than the Kandersteg rockslide, but smaller than the Flims rockslide ( $1.1 \text{ km}^3 < V < 4 \text{ km}^3$ ). This event may have either been undetected so far or may take place in the future. This scenario shifts the rank of the event in constraints 6 and 7 by one (Kandersteg to second and Fernpass to third). As expected, assuming an additional large event at rather late times (3210 BP) results in a slower predicted exhaustion of large events, which is reflected in lower values of the exponent  $\gamma$ .

The third scenario (Fig. 4c) goes a further step ahead by assuming that there was a potential event even larger than the Köfels rockslide, but smaller than the Flims rockslide ( $4 \text{ km}^3 < V < 10 \text{ km}^3$ ) at the time of the Kandersteg rockslide. This means that



**Figure 5.** Cumulative probability of the largest rockslide at the present time (2020 CE). Different line types refer to the three considered scenarios.

210 the rank of the Köfels rockslide in constraint 5 changes from second to third. However, the likelihood values shown in Fig. 4c reveal no further shift towards lower values of  $\gamma$ , but even a small tendency back towards the default scenario (Fig. 4a).

In the following, the rockslide size distributions corresponding to the five dots in all three scenarios (Fig. 4a–c) are considered. This means that the values  $\alpha_V = 1, 1.1, 1.2, 1.3,$  and  $1.4$  are considered for each scenario, while only the most likely values of the other parameters  $\gamma, \mu, n,$  and  $t_0$  are used.

215 Figure 5 shows the cumulative probability of the largest potential rockslide volume at the present time (2020 CE), obtained from the extreme value distribution

$$P(V,t) = 1 - e^{-F(V,t)}. \quad (16)$$

For the default scenario, this volume is greater than  $0.5$  to  $0.7 \text{ km}^3$  (depending on  $\alpha_V$ ) at  $50 \%$  probability (the median). However, the largest rockslide is even larger than the Kandersteg rockslide ( $V = 1.1 \text{ km}^3$ ) at  $10\text{--}20 \%$  probability. While this result seems to contradict constraint 6, we have to keep in mind that the model starts from a power-law distribution at an earlier time  $t_0$  (see contour lines in Fig. 4), which defines the distribution at all later times in combination with the exhaustion model. Looking at Fig. 6, it becomes clear that the median value of the largest volume is close to the volume of the Kandersteg rockslide ( $1.01 < V < 1.13 \text{ km}^3$ ) at its time ( $t = 3210 \text{ BP}$ ), but the respective statistical distribution is not narrow. As an example, the probability that the largest volume is greater than  $2 \text{ km}^3$  is about  $15 \%$  at that time for all considered values of  $\alpha_V$ .

225 While the distribution itself becomes neither narrower nor wider through time, the scenarios scatter increasingly and introduce a larger variability in the expected maximum rockslide sizes.

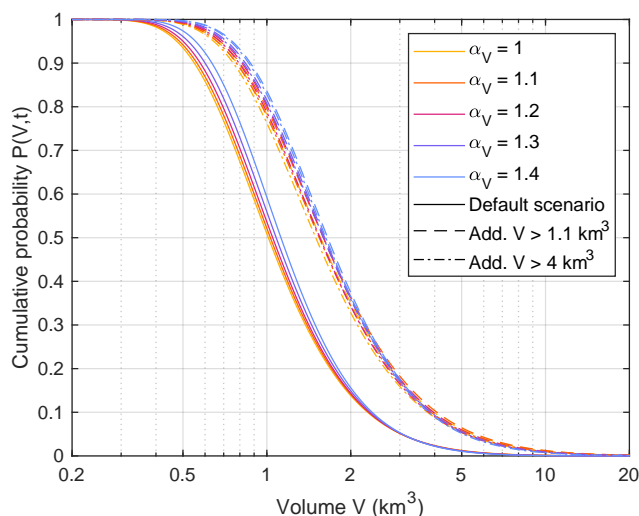


**Figure 6.** Cumulative probability of the largest rockslide at the time of the Kandersteg rockslide (3210 BP). Different line types refer to the three considered scenarios.

As already expected from Fig. 4b,c, the two scenarios with an additional large rockslide that is either undetected or may take place in the future are similar. The median of the largest available volume is in the range between  $0.74 \text{ km}^3$  and  $1.04 \text{ km}^3$  at the present time (Fig. 5).

230 In all scenarios, the probability that a rockslide with  $V \geq 3 \text{ km}^3$  takes place in the future is below 5 %. The probability of a rockslide with  $V \geq 10 \text{ km}^3$  is even lower than 0.2 %. These results shed new light on the conclusion of von Poschinger et al. (2006) that rockslides of several cubic kilometers have to be taken into consideration also at present. Such events may be possible concerning their mechanism and the climatic conditions, but **it is very unlikely that such an event would still be waiting to take place.**

235 In turn, the probability that there will be no rockslide with  $V \geq 0.24 \text{ km}^3$  is also less than 5 % ( $P = 0.95$  in Fig. 5). This result sheds new light on the artificially triggered rockslide that stroke the Vaiont reservoir in 1963 and claimed about 2000 lives. With a volume of about  $0.27 \text{ km}^3$ , this rockslide cannot be considered extraordinarily large, and natural events of this size must be taken into account in the future.

Figure 7 brings the probability of occurrence into play. It shows the expected cumulative frequency  $F(V,t)$  (events per year) at the present time. All curves are strikingly close to each other for  $5 \times 10^5 \text{ m}^3 \leq V \leq 2 \times 10^7 \text{ m}^3$ . In this range, the frequencies are constrained well by recent inventories (constraints 1 and 2).

240 The 100-year event ( $F(V,t) = 0.01 \text{ yr}^{-1}$ ) has a volume of  $4\text{--}4.5 \times 10^7 \text{ m}^3$ . This is approximately the size of the rockslide that took place in Val Pola in 1987 (e.g. Crosta et al., 2003). In the context of large events, the 475-year event is often considered, which is the event with a probability of 10 % over 50 years. The predicted volume of this event is  $0.15\text{--}0.2 \text{ km}^3$ . The predicted frequency of the size of the Vaiont rockslide ( $V = 0.27 \text{ km}^3$ ) is between than  $0.00145 \text{ yr}^{-1}$  and  $0.00085 \text{ yr}^{-1}$ , which means

245

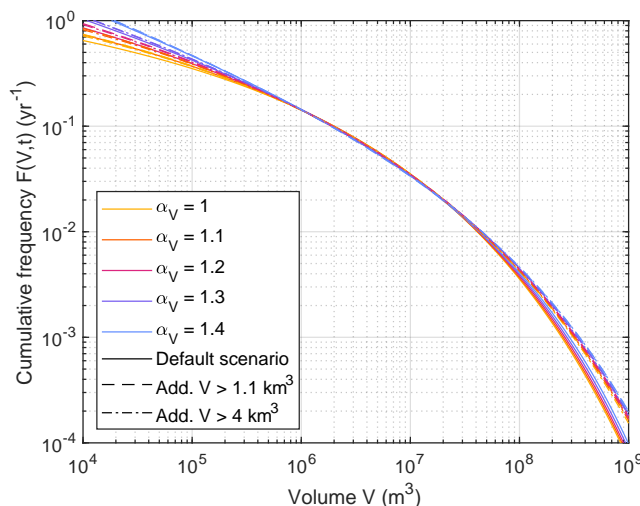


**Figure 7.** Cumulative rockslide frequency at the present time (2020 CE). Different line types refer to the three considered scenarios.

that a 700 to 1200-year event was triggered at the reservoir in 1963. Finally, rockslides with a volume of 1 km<sup>3</sup> should be expected at a probability of less than 1 per 5000 years.

Let us now come back to the question of what we can learn about the process of exhaustion. The likelihood plots shown in Fig. 4 tentatively suggest  $\gamma \approx \frac{1}{3}$ . Despite the uncertainty of this estimate,  $\gamma \approx \frac{1}{3}$  is clearly more likely than  $\gamma \approx \frac{2}{3}$ . In terms of triggering a given site from different points, this finding suggests that triggering should rather take place from the outcrop line of the failure surface (or a part of it) than from any point of the entire failure surface.

This knowledge may also be useful for validating or refuting models. As an example, the model proposed by Hergarten (2012) predicts multiple rockslides with similar volumes at the same location, arising from triggering at different points. The multiplicity of such events as a function of the volume provides a criterion for validation beyond the exponent  $\alpha_V$  of the event-size distribution. The same holds for the more comprehensive model HyLands (Campforts et al., 2020), in which the approach for finding unstable volumes is very similar to that proposed by Hergarten (2012).

As a fundamental property of the process of exhaustion, Fig. 8 shows the  $e$ -folding time

$$T = \frac{1}{\lambda} = \frac{1}{\mu s} = \frac{1}{\mu} \left( \frac{V}{V_0} \right)^{-\gamma}. \quad (17)$$

Since the negative exponent  $\gamma$  of the power-law relation varies between 0.23 and 0.47 among the considered scenarios, there is a considerable scatter in  $T$  at small volumes. For  $V \geq 10 \text{ km}^3$ ,  $T$  is shorter than 2000 yr for all scenarios. In turn,  $T > 65,000 \text{ yr}$  for  $V \leq 1000 \text{ m}^3$ . So paraglacial exhaustion should have a minor effect on the frequency of events with  $V \leq 1000 \text{ m}^3$ . The  $e$ -folding time  $T = 5700 \text{ yr}$  estimated by Cruden and Hu (1993) occurs in Fig. 8 in a range from  $V = 4 \times 10^7 \text{ m}^3$  to  $V = 5 \times 10^8 \text{ m}^3$ , depending on the considered scenario. However, Cruden and Hu (1993) found  $T = 5700 \text{ yr}$  as a lumped  $e$ -folding time for an inventory with  $1000 \text{ m}^3 \leq V \leq 5 \times 10^7 \text{ m}^3$ . So it seems that Cruden and Hu (1993) overestimated the exhaustion of small rockslides (underestimated  $T$ ), perhaps due to undetected potential landslide sites.

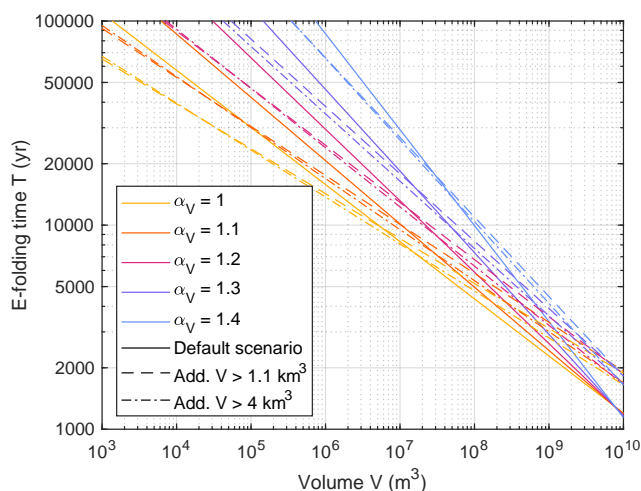


**Figure 8.**  $e$ -folding time of the exhaustion as a function of the volume. Different line types refer to the three considered scenarios.

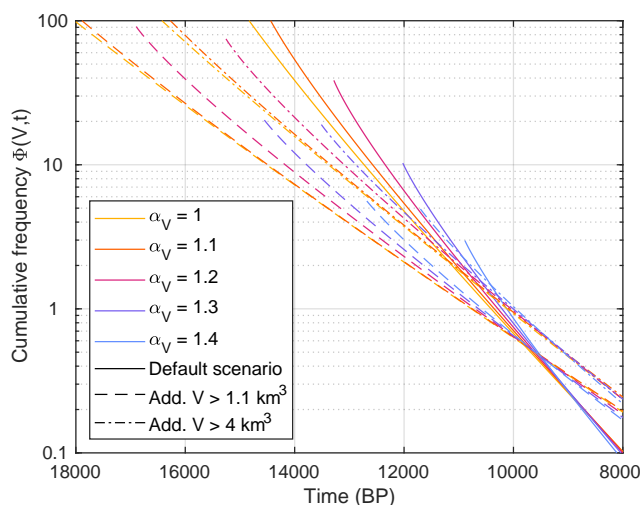


**Figure 9.** Cumulative frequency of potential rockslide sites with  $V \geq 10 \text{ km}^3$ . Different line types refer to the three considered scenarios.

From a geological point of view, the time  $t_0$  at which the process of exhaustion started might even be the most interesting parameter. As shown in Fig. 4, the likely parameter range even comprises values of  $t_0$  earlier than 15000 BP. Such values would bring the deglaciation of the major valleys back into play. However, Fig. 9 reveals that the results become unrealistic between  $t_0$  and the time of the Flims rockslide (9450 BP). In particular for small values of  $\alpha_V$ , the approach predicts an unrealistically large number of rockslides with  $V \geq 10 \text{ km}^3$  during the early phase of exhaustion.

However,  $t_0$  is only a hypothetical time at which exhaustion started from a power-law distribution without any cutoff for large sizes. As observed in Sect. 2, even the quasi-steady state of the DS-FFM already shows a cutoff in the power-law distribution



at large event sizes. This behavior is typical for models in the context of SOC. For the paraglacial exhaustion process, the initial relief imposes an upper limit to the potential rockslide volumes. So we should assume that exhaustion starts later than

275  $t_0$ , but with a distribution of potential volumes that already declines compared to the power law at large volumes. In principle,  $\Phi(V, t)$  should not be much larger than 1 for  $V = 10 \text{ km}^3$  at the time when the process of exhaustion started. If we assume  $1 \leq \Phi(V, t) \leq 2$ , the process of exhaustion should have started between 12000 BP and 10000 BP

In view of this result, the deglaciation of the major valleys cannot only be refuted as an immediate trigger of the huge paraglacial landslides in the Alps, but also as the start of the process of exhaustion. The starting point may, however, be  
280 the massive degradation of permafrost caused by rapid warming in the early Holocene era. For the K fels rockslide, the potential relation to the degradation of permafrost was discussed by Nicolussi et al. (2015) and Zangerl et al. (2021). In these studies, the 2000-year timespan from the beginning of the Holocene era to the rockslide was considered too long for a direct triggering. However, the concept of exhaustion only assumes that the respective sites became potentially unstable when permafrost retreated. From the statistical data, a time span of 2000 yr to the occurrence of an actual instability is not too long

285 However, the question for the actual trigger for the respective rockslides remains open. In principle, even the question whether a unique trigger is needed is still open. Large instabilities may also develop slowly (e.g., Riva et al., 2018; Spreafico et al., 2021) and failure may finally occur without a unique trigger.

## 5 Conclusions

In this study, a theoretical concept for event-size dependent exhaustion was developed. The process starts from a given set of  
290 potential events, which are randomly triggered through time. In contrast to a previous approach (Cruden and Hu, 1993), the probability of triggering depends on event size.

The concept was applied to paraglacial rockslides in the European Alps. Although available inventories cover only a quite short time span and older data are limited to a few huge rockslides, constraining the parameters involves a large uncertainty. Nevertheless, some fundamental results could be obtained.

295 Assuming that the probability of triggering is related to the volume  $V$  by a power law  $V^\gamma$ , the results indicate exponents  $\gamma \approx \frac{1}{3}$  or even slightly lower. Interpreting the dependence on volume as the possibility to initiate an event from different points, this result suggests that initiation may rather start from the outcrop line of the failure surface (or from a part of this line) than from any point of the failure surface. The exponent  $\gamma$  may be helpful for validating or refuting statistical or process-based models.

300 The concept of event-size dependent exhaustion predicts an exponential decrease of rockslide frequency through time with a decay constant depending on  $V$ . For small rockslides with  $V \leq 1000 \text{ m}^3$ , the respective  $e$ -folding time is longer than 65,000 yr. So the frequency of small rockslides should not have decreased much since the last glaciation. In turn, the predicted  $e$ -folding time is shorter than 2000 yr for  $V \geq 10 \text{ km}^3$ . So the occurrence of rockslides in the order of magnitude of the Flims rockslide is unlikely at present times. These  $e$ -folding times are, however, consistent with the idea that the process of exhaustion was  
305 initiated by the degradation of permafrost at the beginning of the Holocene epoch.



For the largest rockslide possible at present times, different considered scenarios predict a median volume of 0.5 to 1 km<sup>3</sup>. However, the predicted frequency of such large events is low (less than 1 per 5000 years for  $V \geq 1$  km<sup>3</sup>). The predicted 100-year event has a volume of  $4\text{--}4.5 \times 10^7$  m<sup>3</sup>. The artificially triggered rockslide at the Vaiont reservoir (1963 CE,  $V = 0.27$  km<sup>3</sup>) can be considered a 700 to 1200-year event in this context.

310 *Code and data availability.* All codes are available in a Zenodo repository at <https://doi.org/10.5281/zenodo.7313868> (Hergarten, 2022). This repository also contains the data obtained from the numerical simulations. The author is happy to assist interested readers in reproducing the results and performing subsequent research.

### Appendix A: The maximum likelihood formalism

In this section, a maximum likelihood approach that combines data of the two types discussed in Sect. 4 is developed.

315 The first type of data (constraints 1–3 in Sect. 4) refers to the number of events in a given range of sizes  $[s_1, s_2]$  during a given time interval  $[t_1, t_2]$ . The expected number  $N$  easily obtained from the cumulative frequency  $\Phi(s, t)$  of the potential events (Eq. 8) as

$$N = \Phi(s_1, t_1) - \Phi(s_2, t_1) - \Phi(s_1, t_2) + \Phi(s_2, t_2). \quad (\text{A1})$$

Then the likelihood is given by the Poisson distribution

320 
$$L = \frac{N^n}{n!} e^{-N}, \quad (\text{A2})$$

where  $n$  is the actual number.

The second type of data (constraints 4–7 in Sect. 4) is described by rank-ordering statistics. The probability density of the  $k^{\text{th}}$  largest among  $n$  events is

$$p_k(s) = \binom{n}{k} \left(1 - \int_s^\infty p(\sigma) d\sigma\right)^{n-k} \binom{k}{1} p(s) \left(\int_s^\infty p(\sigma) d\sigma\right)^{k-1} \quad (\text{A3})$$

325 (Sornette, 2000, Eq. 6.4), where  $p(s)$  is the probability density of the events. Replacing  $p(s)$  by the frequency density  $\phi(s) = np(s)$ , switching to the cumulative frequency  $\Phi(s)$ , and joining the binomial coefficients yields


$$p_k(s) = \frac{(n-1)!}{(n-k)!(k-1)!} \left(1 - \frac{\Phi(s)}{n}\right)^{n-k} \phi(s) \left(\frac{\Phi(s)}{n}\right)^{k-1}. \quad (\text{A4})$$

In the limit  $n \rightarrow \infty$  at finite  $k$ , terms  $n-1, \dots, n-k$  can be replaced by  $n$ . In combination with the relation  $(1 - \frac{x}{n})^n \rightarrow e^{-x}$ , we obtain

330 
$$p_k(s) = \frac{1}{(k-1)!} e^{-\Phi(s)} \Phi(s)^{k-1} \phi(s). \quad (\text{A5})$$






When using the maximum likelihood method, we must keep in mind that the measured event size is  $V$ , while the relation between  $s$  and  $V$  (Eq. 13) contains one of the parameters ( $\gamma$ ) to be estimated. Therefore, we must transform the probability density  $p_k$  (and thus  $\phi$ ) from  $s$  to  $V$ . For this purpose, we need the derivative 

$$\frac{ds}{dV} = V_0^{-\gamma} \gamma V^{\gamma-1} = \frac{\gamma}{V_0} s^{\frac{\gamma-1}{\gamma}} \quad (\text{A6})$$

335 and obtain

$$L = \frac{1}{(k-1)!} e^{-\Phi(s)} \Phi(s)^{k-1} \phi(s) \frac{\gamma}{V_0} s^{\frac{\gamma-1}{\gamma}} \quad (\text{A7})$$

for the respective likelihood. Finally, the total likelihood is the product of the likelihood values according to Eq. (A2) for the constraints 1–3 and Eq. (A7) for the constraints 1–4 

*Competing interests.* The author declares that there is no conflict of interest.



## 340 References

- Aaron, J., Wolter, A., Loew, S., and Volken, S.: Understanding failure and runout mechanisms of the Flims rockslide/rock avalanche, *Front. Earth Sci.*, 8, 224, <https://doi.org/10.3389/feart.2020.00224>, 2020.
- Alvioli, M., Guzzetti, F., and Rossi, M.: Scaling properties of rainfall induced landslides predicted by a physically based model, *Geomorphology*, 213, 38–47, <https://doi.org/10.1016/j.geomorph.2013.12.039>, 2014.
- 345 Bak, P., Tang, C., and Wiesenfeld, K.: Self-organized criticality. An explanation of  $1/f$  noise, *Phys. Rev. Lett.*, 59, 381–384, <https://doi.org/10.1103/PhysRevLett.59.381>, 1987.
- Ballantyne, C. K.: A general model of paraglacial landscape response, *Holocene*, 12, 371–376, <https://doi.org/10.1191/0959683602hl553fa>, 2002a.
- Ballantyne, C. K.: Paraglacial geomorphology, *Quat. Sci. Rev.*, 21, 1935–2017, [https://doi.org/10.1016/S0277-3791\(02\)00005-7](https://doi.org/10.1016/S0277-3791(02)00005-7), 2002b.
- 350 Bennett, G. L., Molnar, P., Eisenbeiss, H., and McArdeell, B. W.: Erosional power in the Swiss Alps: characterization of slope failure in the Illgraben, *Earth Surf. Process. Landforms*, 37, 1627–1640, <https://doi.org/10.1002/esp.3263>, 2012.
- Brunetti, M. T., Guzzetti, F., and Rossi, M.: Probability distribution of landslide volumes, *Nonlin. Processes Geophys.*, 16, 179–188, <https://doi.org/10.5194/npg-16-179-2009>, 2009.
- Campforts, B., Shobe, C. M., Steer, P., Vanmaercke, M., Lague, D., and Braun, J.: HyLands 1.0: a hybrid landscape evolution model  
355 to simulate the impact of landslides and landslide-derived sediment on landscape evolution, *Geosci. Model Dev.*, 13, 3863–3886, <https://doi.org/10.5194/gmd-13-3863-2020>, 2020.
- Christensen, K., Flyvbjerg, H., and Olami, Z.: Self-organized critical forest-fire model: mean-field theory and simulation results in 1 to 6 dimensions, *Phys. Rev. Lett.*, 71, 2737–2740, <https://doi.org/10.1103/PhysRevLett.71.2737>, 1993.
- Clar, S., Drossel, B., and Schwabl, F.: Scaling laws and simulation results for the self-organized critical forest-fire model, *Phys. Rev. E*, 50,  
360 1009–1018, <https://doi.org/10.1103/PhysRevE.50.1009>, 1994.
- Crosta, G. B., Imposimato, S., and Roddeman, D. G.: Numerical modelling of large landslides stability and runout, *Nat. Hazards Earth Syst. Sci.*, 3, 523–538, <https://doi.org/10.5194/nhess-3-523-2003>, 2003.
- Cruden, D. M. and Hu, X. Q.: Exhaustion and steady state models for predicting landslide hazards in the Canadian Rocky Mountains, *Geomorphology*, 8, 279–285, [https://doi.org/10.1016/0169-555X\(93\)90024-V](https://doi.org/10.1016/0169-555X(93)90024-V), 1993.
- 365 Densmore, A. L., Ellis, M. A., and Anderson, R. S.: Landsliding and the evolution of normal-fault-bounded mountains, *J. Geophys. Res.*, 103, 15 203–15 219, <https://doi.org/10.1029/98JB00510>, 1998.
- Deplazes, G., Anselmetti, F. S., and Hajdas, I.: Lake sediments deposited on the Flims rockslide mass: the key to date the largest mass movement of the Alps, *Terra Nova*, 19, 252–258, <https://doi.org/10.1111/j.1365-3121.2007.00743.x>, 2007.
- Drossel, B. and Schwabl, F.: Self-organized critical forest-fire model, *Phys. Rev. Lett.*, 69, 1629–1632,  
370 <https://doi.org/10.1103/PhysRevLett.69.1629>, 1992.
- Grassberger, P.: On a self-organized critical forest fire model, *J. Phys. A*, 26, 2081–2089, <https://doi.org/10.1088/0305-4470/26/9/007>, 1993.
- Gruner, U.: Bergstürze und Klima in den Alpen – gibt es Zusammenhänge?, *Bull. angew. Geol.*, 11, 25–34, <https://doi.org/10.5169/seals-226166>, 2006.
- Hartmeyer, I., Delleske, R., Keuschnig, M., Krautblatter, M., Lang, A., Schrott, L., and Otto, J.-C.: Current glacier recession causes  
375 significant rockfall increase: the immediate paraglacial response of deglaciating cirque walls, *Earth Surf. Dynam.*, 8, 729–751, <https://doi.org/10.5194/esurf-8-729-2020>, 2020.



- Henley, C. L.: Statics of a “self-organized” percolation model, *Phys. Rev. Lett.*, 71, 2741–2744, <https://doi.org/10.1103/PhysRevLett.71.2741>, 1993.
- Hergarten, S.: Topography-based modeling of large rockfalls and application to hazard assessment, *Geophys. Res. Lett.*, 39, L13 402, <https://doi.org/10.1029/2012GL052090>, 2012.
- 380 Hergarten, S.: Event-size dependent exhaustion and paraglacial rockslides, <https://doi.org/10.5281/zenodo.7313868>, 2022.
- Hergarten, S. and Krenn, R.: A semi-phenomenological approach to explain the event-size distribution of the Drossel-Schwabl forest-fire model, *Nonlin. Processes Geophys.*, 18, 381–388, <https://doi.org/10.5194/npg-18-381-2011>, 2011.
- Hergarten, S. and Neugebauer, H. J.: Self-organized criticality in a landslide model, *Geophys. Res. Lett.*, 25, 801–804, <https://doi.org/10.1029/98GL50419>, 1998.
- 385 Hovius, N., Stark, C. P., and Allen, P. A.: Sediment flux from a mountain belt derived by landslide mapping, *Geology*, 25, 231–234, [https://doi.org/10.1130/0091-7613\(1997\)025<0231:SFFAMB>2.3.CO;2](https://doi.org/10.1130/0091-7613(1997)025<0231:SFFAMB>2.3.CO;2), 1997.
- Ivy-Ochs, S., Kerschner, H., Reuther, A., Preusser, F., Heine, K., Maisch, M., Kubik, P. W., and Schlüchter, C.: Chronology of the last glacial cycle in the European Alps, *J. Quaternary Sci.*, 23, 559–573, <https://doi.org/10.1002/jqs.1202>, 2008.
- 390 Jeandet, L., Steer, P., Lague, D., and Davy, P.: Coulomb mechanics and relief constraints explain landslide size distribution, *Geophys. Res. Lett.*, 46, 4258–4266, <https://doi.org/10.1029/2019GL082351>, 2019.
- Jensen, H. J.: *Self-Organized Criticality – Emergent Complex Behaviour in Physical and Biological Systems*, Cambridge University Press, Cambridge, New York, Melbourne, 1998.
- Krenn, R. and Hergarten, S.: Cellular automaton modelling of lightning-induced and man made forest fires, *Nat. Hazards Earth Syst. Sci.*, 9, <https://doi.org/10.5194/nhess-9-1743-2009>, 2009.
- 395 Lari, S., Frattini, P., and Crosta, G. B.: A probabilistic approach for landslide hazard analysis, *Engin. Geol.*, 182, 3–14, <https://doi.org/10.1016/j.enggeo.2014.07.015>, 2014.
- Liucci, L., Melelli, L., Suteanu, C., and Ponziani, F.: The role of topography in the scaling distribution of landslide areas: A cellular automata modeling approach, *Geomorphology*, 290, 236–249, <https://doi.org/10.1016/j.geomorph.2017.04.017>, 2017.
- 400 Malamud, B. D., Morein, G., and Turcotte, D. L.: Forest fires: an example of self-organized critical behavior, *Science*, 281, 1840–1842, <https://doi.org/10.1126/science.281.5384.1840>, 1998.
- Malamud, B. D., Turcotte, D. L., Guzzetti, F., and Reichenbach, P.: Landslide inventories and their statistical properties, *Earth Surf. Process. Landforms*, 29, 687–711, <https://doi.org/10.1002/esp.1064>, 2004.
- Mohadjer, S., Ehlers, T. A., Nettesheim, M., Ott, M. B., Glotzbach, C., and Drews, R.: Temporal variations in rockfall and rock-wall retreat rates in a deglaciated valley over the past 11 ky, *Geology*, 48, 594–598, <https://doi.org/10.1130/G47092.1>, 2020.
- Nicolussi, K., Spötl, C., Thurner, A., and Reimer, P. J.: Precise radiocarbon dating of the giant Kofels landslide (Eastern Alps, Austria), *Geomorphology*, 243, 87–91, <https://doi.org/10.1016/j.geomorph.2015.05.001>, 2015.
- Pastor-Satorras, R. and Vespignani, A.: Corrections to scaling in the forest-fire model, *Phys. Rev. E*, 61, 4854–4859, <https://doi.org/10.1103/physreve.61.4854>, 2000.
- 410 Pruessner, G. and Jensen, H. J.: Broken scaling in the forest-fire model, *Phys. Rev. E*, 65, 056 707, <https://doi.org/10.1103/PhysRevE.65.056707>, 2002.
- Riva, F., Agliardi, F., Amitrano, D., and Crosta, G. B.: Damage-based time-dependent modeling of paraglacial to postglacial progressive failure of large rock slopes, *J. Geophys. Res. Earth Surf.*, 123, 124–141, <https://doi.org/10.1002/2017JF004423>, 2018.



- Schenk, K., Drossel, B., and Schwabl, F.: Self-organized critical forest-fire model on large scales, *Phys. Rev. E*, 65, 026135, 415  
<https://doi.org/10.1103/PhysRevE.65.026135>, 2002.
- Singeisen, C., Ivy-Ochs, S., Wolter, A., Steinemann, O., Akçar, N., Yesilyurt, S., and Vockenhuber, C.: The Kandersteg rock avalanche (Switzerland): integrated analysis of a late Holocene catastrophic event, *Landslides*, 17, 1297–1317, <https://doi.org/10.1007/s10346-020-01365-y>, 2020.
- Sornette, D.: *Critical Phenomena in Natural Sciences – Chaos, Fractals, Selforganization and Disorder: Concepts and Tools*, Springer, Berlin, 420 Heidelberg, New York, 2000.
- Spreafico, M. C., Sternai, P., and Agliardi, F.: Paraglacial rock-slope deformations: sudden or delayed response? Insights from an integrated numerical modelling approach, *Landslides*, 18, 1311–1326, <https://doi.org/10.1007/s10346-020-01560-x>, 2021.
- Strunden, J., Ehlers, T. A., Brehm, D., and Nettesheim, M.: Spatial and temporal variations in rockfall determined from TLS measurements in a deglaciated valley, Switzerland, *J. Geophys. Res. Earth Surf.*, 120, 1251–1273, <https://doi.org/10.1002/2014JF003274>, 2015.
- 425 Tanyas, H., Allstadt, K. E., and van Westen, C. J.: An updated method for estimating landslide-event magnitude, *Earth Surf. Process. Landforms*, 43, 1836–1847, <https://doi.org/10.1002/esp.4359>, 2018.
- Tebbens, S. F.: Landslide scaling: A review, *Earth Space Sci.*, 7, e2019EA000662, <https://doi.org/10.1029/2019EA000662>, 2020.
- Valagussa, A., Frattini, P., and Crosta, G. B.: Earthquake-induced rockfall hazard zoning, *Engin. Geol.*, 182, 213–225, <https://doi.org/10.1016/j.enggeo.2014.07.009>, 2014.
- 430 von Poschinger, A., Wassmer, P., and Maisch, M.: The Flims rockslide: history of interpretation and new insights, in: *Landslides from Massive Rock Slope Failure*, edited by Evans, S. G., Scarascia-Mugnozza, G., Strom, A., and Hermanns, R. L., pp. 329–356, Springer, Dordrecht, [https://doi.org/10.1007/978-1-4020-4037-5\\_18](https://doi.org/10.1007/978-1-4020-4037-5_18), 2006.
- Zangerl, C., Schneeberger, A., Steiner, G., and Mergili, M.: Geographic-information-system-based topographic reconstruction and geomechanical modelling of the Kofels rockslide, *Nat. Hazards Earth Syst. Sci.*, 21, 2461–2483, <https://doi.org/10.5194/nhess-21-2461-2021>, 435 2021.
- Zinck, R. D. and Grimm, V.: More realistic than anticipated: A classical forest-fire model from statistical physics captures real fire shapes, *Open Ecol. J.*, 1, 8–13, <https://doi.org/10.2174/1874213000801010008>, 2008.